ACS APPLIED MATERIALS & INTERFACES

Research Article

www.acsami.org

Surface Modification with Dopamine and Heparin/Poly-L-Lysine Nanoparticles Provides a Favorable Release Behavior for the Healing of Vascular Stent Lesions

Tao Liu,[†] Zheng Zeng,[†,‡] Yang Liu,[†] Jian Wang,[†] Manfred F. Maitz,[†,§] Yuan Wang,[†] Shihui Liu,[†,∥] Junying Chen,*[,†] and Nan Huang[†]

[†]Key Laboratory of Advanced Technology of Materials, Ministry of Education, Southwest Jiaotong University, Chengdu 610031, PR China

[‡]School of Life Science and Technology, Southwest Jiaotong University, Chengdu 610031, P.R. China

[§]Max Bergmann Center of Biomaterials, Leibniz Institute of Polymer Research Dresden, Hohe Strasse 06, 01069 Dresden, Germany

[∥]Naton Institute of Medical Technology, Naton Medical Group, Peking 100082, P. R. China

ABSTRACT: Surface biofunctional modification of coronary artery stents to prevent thrombosis and restenosis formation, as well as accelerate endothelialization, has become a new hot spot. However, bioactive coatings on implants are not yet sufficiently developed for long-term activity, as they quickly lose efficiency in vivo and finally fail. On the basis of a novel time-ordered concept of biofunctionality for vascular stents, heparin/poly L-lysine nanoparticle (NP) was developed and immobilized on a polydopamine-coated titanium surface, with the aim of regulating and maintaining the intravascular biological response within the normal range after biomaterial implantation. An in vitro dynamic release model was established to mimic the blood flow condition in vivo with three phases: (1) An early phase (1−7 days) with release of predominantly anticoagulant and anti-inflammatory substances and to a minor degree antiproliferative effects against smooth muscle cells (SMCs); (2) this is followed by a phase (7−14 days) of supported endothelial cell (ECs) proliferation and suppressed SMC proliferation with persisting high antithrombogenicity and anti-inflammatory properties of the surface. (3) Finally, a stable stage (14−28 days) with adequate biomolecules on the surface that maintain hemocompatibility and anti inflammation as well as inhibit SMCs proliferation and promote ECs growth. In vivo animal tests further confirmed that the NP-modified surface provides a favorable release behavior to apply a stage-adjusted remedy. We suggested that these observations provide important guidance and potential means for reasonable and suitable platform construction on a stent surface.

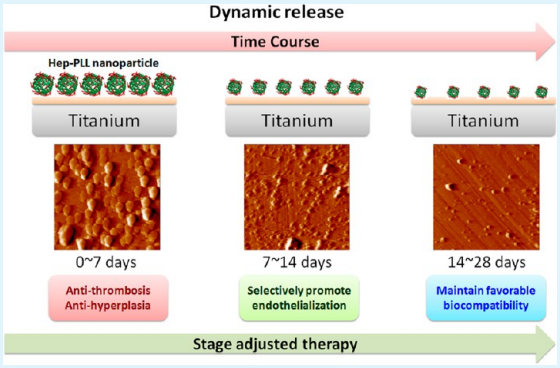

KEYWORDS: *heparin, nanoparticle, endothelial cell, thrombosis, restenosis*

1. INTRODUCTION

Percutaneous coronary intervention (PCI) using metal stents is the main approach for coronary artery disease (CVD) therapy. The main advantage of PCI is the low surgical risk and the short recovery time. However, according to clinical results, traditional bare metal stents present comparable rates of adverse cardiac events and even higher rates of repeated revascularization compared with coronary artery bypass graft (CABG) surgery due to nonadjusted mechanical properties and biocompatibility of the materials.[1,2] Although the emergence of drug-eluting stents (DESs) with the aim of resolving in-stent restenosis has triggered a revolution in interventional cardiology, side effects, such as inflammation, late thrombosis, and late restenosis, still remain.

After PCI, the pathological evolution of the implantation site in response to a bare metal coronary artery stent is time-ordered and can be divided into three stages: (1) An early stage within one month after stent implantation with the risks of acute and subacute stent thrombosis. Acute thrombosis usually occurs within a few minutes to hours, whereas subacute thrombosis occurs within a few days to a month, and the highest risk period is in the first week.[3,4] Then, induced by the mechanical vascular injury, leukocytes are recruited and infiltrate the site of the denuded endothelium layer with aggregated and activated blood platelets.[5] The inflammatory reaction usually occurs within a few days to weeks, and the highest risk is also in the first week.[5,6] Induced by the above-described pathological processes, the intimal cell proliferation rate reaches its highest level within 3−7 days, and the intimal thickness significantly increases within 4 weeks.[7−9] (2) In the middle phase, from 1−3 months, the stent surface is still exposed to the blood flow, but starts to be covered by the

Received: March 13, 2014
Accepted: April 14, 2014
Published: April 14, 2014

   dx.doi.org/10.1021/am5015309 | ACS Appl. Mater. Interfaces 2014, 6, 8729−8743

surrounding tissue; however, delayed or incomplete endothelialization raises the risk of thrombosis and restenosis. (3) In the late stage after 3 months, the stent is generally considered embedded in the vascular tissue, but adverse material−tissue interactions may be a reason for late thrombosis and restenosis.

For stent design, it is important to consider this time-ordered pathological evolution and to apply a stage-adjusted remedy. A reasonable modification of the stent surface should meet the following requirements: (1) prevent thrombosis formation and inflammatory reaction at stage 1, inhibit the excessive proliferation of smooth muscle cells (SMCs), and prevent intimal hyperplasia; (2) accelerate endothelialization at the early stage to improve the formation of the confluent endothelium layer on the stent surface within 1 month to decrease or eliminate the adverse events at stage 2, and (3) the exposed surface after complete elution of the drug should be biocompatible to avoid adverse material−tissue interface interactions.

Unfortunately, the currently applied DESs do not exhibit such time-ordered activity. The delayed endothelium regeneration caused by antiproliferative drugs and the persistence of polymer coatings may raise the incidence of adverse cardiac events in stages 2 and 3, respectively. Biodegradable polymer[10,11] and polymer-free DES[12,13] have been developed to reduce the polymer-associated incompatibility. However, the degradation products of biodegradable polymers may increase the occurrence of inflammatory reactions and subsequently cause intimal hyperplasia at stage 2, and the exposed material surface after the complete degradation of the polymer may also cause restenosis and late thrombosis at stage 3. For polymer-free DES, in addition to the adverse interface reaction problem, it is difficult to control the release kinetics of antiproliferative drugs to within a certain range.

At present, the major challenge faced in the surface modification of stents lies in the simultaneous prevention of intimal hyperplasia and promotion of endothelium regeneration. The traditionally used antiproliferative drugs, such as paclitaxel, sirolimus, and its derivatives, tend to discourage endothelial cell (EC) proliferation. The combinatory application of antiproliferative and endothelium stimulating drugs presents no benefit.[13−15] Therefore, other drugs and methods are needed for stent surface modification to selectively inhibit intimal hyperplasia and promote EC proliferation, and heparin may be a potential candidate. In addition to being a widely used anticoagulant, heparin is frequently used clinically for anti-inflammation therapy and exhibits a significant inhibitory effect on SMC proliferation and migration.[16−18] Moreover, the specific affinity of angiogenesis-related cytokines to heparin makes accelerated endothelialization by surface heparinization possible. Therefore, heparin-coated stents have emerged, but their application remains limited for the prevention of thrombosis and intimal hyperplasia.[19,20] An overdosage of heparin and a loss of drug release control may delay endothelium regeneration and increase the occurrence of adverse events at stage 2.[21]

To meet the requirement of time-ordered response by a surface modification, the heparin density and release behavior should be precisely controlled within a certain range. In the present study, a novel heparin/poly-L-lysine (Hep/PLL) nanoparticle has been developed and immobilized on a dopamine-coated Ti surface to attain a heparinized surface with high biological function and time-ordered potential. According to our previous research,[22] modification of the concentration ratio of heparin to PLL was found to influence the immobilized heparin density and release behavior. On the basis of a comprehensive consideration of the biocompatibility and time-ordered biofunctional requirements, a specific Hep/PLL nanoparticle was finally worked out as the optimal composition. The major advantages of a surface with immobilized Hep/PLL nanoparticle are high anticoagulant activity, selective inhibition of SMCs, and promotion of EC proliferation. In this study, the time-ordered potential of this nanoparticle-modified surface has been further demonstrated in a dynamic release model, and the change in the biological function of the surface at different time points of the pathological evolution in stage 1 was investigated. In combination with in vivo animal tests, we have demonstrated that the NP-modified surface presents an adequate time-ordered biofunction to selectively direct an intravascular biological response.

2. EXPERIMENTAL SECTION

2.1. Materials and Reagents. Ti substrate material was cut into round disks (Ø 10 mm) and mirror-polished before use. Dopamine (DM) and poly-L-lysine (PLL, MW 150−300 kDa), toluidine blue O (TBO), and acid orange II (AO II) were purchased from Sigma-Aldrich. Heparin sodium (Hep, MW < 8KDa) was purchased from Shanghai Bio science and technology company. Rhodamine, mouse monoclonal anti human p-selectin antibody, rabbit monoclonal anti human vWF antibody and 4′,6-diamidino-2-phenylindole (DAPI) were purchased from Sigma-Aldrich. Mouse TNF-α and IL-6 ELISA kits, rabbit monoclonal anti human α-SMA antibody, fluorescein isothiocyanate (FITC)-conjugated goat anti rabbit IgG antibody and FITC-conjugated goat anti mouse IgG antibody were purchased from Boster Biological Technology (Wuhan, China). Mouse monoclonal anti human AT III antibody, horseradish peroxidase (HRP)-conjugated goat anti mouse IgG antibody and TMB (3,3′,5,5′ tetramethylbenzidene) color developing agent were purchased from BD Bioscience (San Jose, CA). Mouse monoclonal anti human fibrinogen (FGN) and FGN γ chain antibody were purchased from Abcam (UK). 0.01 M phosphate buffered saline (PBS, pH 7.4) was used as PLL and Hep solution medium and heparin release medium.

2.2. Hep/PLL Nanoparticle Preparation and Characterization. First, 5 mg/mL Hep solution (in PBS, pH 7.4) was prepared and sterile-filtered, and 0.5 mg/mL PLL was aseptically prepared; both Hep and PLL solution were stored at 4 °C sterile sealed until use. For Hep/PLL nanoparticle preparation, Hep and PLL solution were warmed to 37 °C, and then an equal volume of heparin solution was dropwise added to the PLL solution, and the mixture was subsequently homogenized by ultrasonic treatment for 5 min.

The mean size, particle dispersion index (PDI), and zeta potential of the prepared NP were determined by dynamic light scattering (DLS) using a ZETA-SIZER, MALVERN Nano-2S90 (Malvern Ltd., Malvern, UK). Each measurement was repeated three times. The morphology of the particles was examined by transmission electron microscopy (Tecnai G2 F20 S-TWIN, FEI). Briefly, the nanoparticles were precipitated from suspension by high speed centrifugation (15,000 rpm, 10 min), the supernatant was discarded to remove free heparin and the precipitated nanoparticles were resuspended in PBS. Ten μL of the purified TEM sample was placed on a copper grid with a carbon-coated Formvar film. A few minutes after the deposition, the excess solution was removed with a strip of filter paper. The sample was then dried at room temperature and examined by TEM.

2.3. Hep/PLL Nanoparticle Immobilization and Dynamic Release. The prepared NPs were immobilized on dopamine (DM) coated Ti surface. First, Ti coupons were immersed into the prepared 2 mg/mL DM solution (in Tris buffer, pH 8.5) and incubated at 20 °C under static conditions for 12 h, then the samples were thoroughly sonicated in ultra pure (UP) water and marked as layer one. The second and the third DM layer were grafted by repeated incubation and sonication. Subsequently, 500 μL of NP suspension was added to

each sample and incubated at 37 °C for 24 h under mild shaking. Ultimately, the samples were thoroughly rinsed with PBS and UP water.

Heparin release from the nanoparticle immobilized samples was determined in a medium of sterile-filtered PBS (pH 7.4) containing 0.01% NaN_3. Briefly, the samples was placed in airtight centrifuge tubes with 1.5 mL medium, and incubated at 37 °C under constant rotation (60−65 rpm) for 1, 3, 5, 7, 10, 14, 21, and 28 days.

2.4. FTIR. The development of surface chemical group composition during heparin release was determined by Fourier transform infrared spectroscopy (FTIR) (NICOLET 5700 infrared spectroscopy, USA) with the model of diffuse reflectance. Scanning was conducted in the range from 400 to 4000 cm^{-1}.

2.5. XPS. X-ray photoelectron spectroscopy (XPS) (Kratos Ltd., UK) analysis was performed on an AXIS His spectrometer with a monochromatic Al Kα X-ray source (1486.6 eV photons, 150W) to investigate the element composition change of the surfaces during heparin release. The pressure in the chamber was below 2×10^{-9} Torr, the binding energy scale was referenced by setting C_{1s} peak at 284.6 eV.

2.6. AFM. The changes of surface topography during release were determined by Nanowizard II atom force microscopy (AFM) (JPK Instruments, Berlin, Germany) in contact mode at room temperature with subsequent image analysis using CSPM Imager software. Before AFM analysis, the samples were rinsed twice with UP water and the surface was carefully blown dry.

2.7. Water Contact Angle. The hydrophilicity alteration of the surfaces during release was determined by measuring the static water contact angle using a Krüss GmbH DSA100 Mk 2 goniometer at room temperature. A droplet of UP water was added to the dried surface, and then the contact angle was calculated by a circle segment function of the DSA 1.8 software. At least three different sites were taken into measurement for each sample.

2.8. Quantitative Characterization of Heparin Residual Density and Release Amount. during release, the residual heparin density of the different sample surfaces at each time point was quantified by a modified toluidine blue O (TBO) assay according to Smith et al.[23] Briefly, the samples were immersed in a 0.04 wt % TBO/0.01 M HCl/0.2 wt % NaCl aqueous solution and incubated at 37 °C for 4 h, then the TBO solution was removed and the samples were thoroughly rinsed with UP water. Subsequently, the samples were immersed in 2 mL of 80% ethanol/0.1 M NaOH mixture (v/v: 4/1) solution to dissolve the Hep-TBO complex. The absorbance of the eluate was measured at 530 nm and calibrated to the heparin amount at a standard curve. The calibration standard curve was prepared as following: 2 mL of TBO solution was added to 2 mL of known concentration heparin solution (in PBS, pH 7.4) and then the mixture was incubated at 37 °C for 4 h with gently shaking. The mixture was then centrifuged at 3500 rpm for 10 min, and the Hep/TBO precipitate was carefully rinsed with aqueous 0.01 M HCl/0.2 wt % NaCl. Subsequently, the Hep/TBO precipitate was dissolved in 2 mL of 80% ethanol/0.1 M NaOH mixture (v/v: 4/1) solution and the absorbance was measured at 530 nm.

For heparin release assay, 1 mL of the release medium at different time points was collected and 1 mL of TBO solution was added. After incubation at 37 °C for 4 h, the Hep/TBO precipitate was centrifuged and detected by using a same procedure of standard curve preparation.

2.9. Quantitative Characterization of the Residual Amine Density. The change of the exposed amine density during release was determined by modified acid orange II (AO II) assay according to Hamerli et al.[24] Briefly, the samples were incubated in 1 mL of 0.5 mM AO II in HCl solution (pH 3) at 37 °C for 6 h and then rinsed thoroughly with HCl solution. The excess solution was subsequently absorbed by filter paper and the samples were immersed into 1 mL NaOH solution (pH 10) with gently shaking for 15 min. The absorbance of the eluate was measured at 485 nm and calibrated at a standard curve of defined AO II concentrations.

2.10. Blood Compatibility Evaluation. After different release periods, the samples were collected and the blood compatibility was evaluated. Fresh citrate anticoagulated human whole blood used in blood compatibility evaluation was obtained from Chengdu Blood Center, China, following the legal rules for work with human material. The experiment was performed within 12 h after the blood donation.

2.10.1. Platelet Adhesion and Activation. The changes of surface blood compatibility during heparin release were evaluated by in vitro platelet adhesion and activation. Platelet-rich plasma (PRP) was first separated from fresh human whole blood by centrifugation at 1500 rpm for 15 min. Fifty microliters of PRP was then added to sample surfaces and incubated at 37 °C. After 1 h, the samples were gently rinsed 3 times with PBS and subsequently used for lactate dehydrogenase (LDH) assay, p-selectin assay and immunofluorescence staining, respectively.

The LDH assay was used to quantify the amount of adherent platelets on different sample surfaces. Briefly, 50 μL of 1% Triton X-100 was added to sample surfaces and incubated at 37 °C, after 5 min, 25 μL of lysate were transferred from each surface and mixed with 200 μL tris (hydroxymethyl) aminomethane base buffer mixture containing 0.28 mg/mL nicotinamide adenine dinucleotide (NADH) and 0.187 mg/mL pyruvate in a 96-well plate. Subsequently, the absorbance was measured in a microplate reader at 340 nm. The released LDH activity from the adherent platelets on sample surfaces was calibrated at a calibration curve of a defined concentration of lysed platelets.

The p-selectin expression was quantified to evaluate the activation degree of adherent platelets on the different surfaces. First, 30 μL of mouse monoclonal antihuman p-selectin antibody (first antibody) was added to each sample surface and incubated at 37 °C for 1 h. The samples were then rinsed 3 times with PBS and incubated in goat serum at 37 °C for 1 h to block nonspecific adsorption. Subsequently, 30 μL of HRP-conjugated goat anti mouse IgG antibody (second antibody) wasadded. After rinsed 3 times with PBS, 100 μL of TMB agent was added to each surface and incubated at room temperature for 10 min under dark condition, and 50 μL of 1 M H_2SO_4 was then added to each sample to stop the color reaction. Ultimately, 100 μL of reaction solution was transferred from the surface into a 96-well plate and the absorbance was measured at 450 nm.

P-selectin immunofluorescence staining was prepared to observe the platelet adhesion and activation profile visually. The samples were first fixed in 4% paraformaldehyde for 12 h at room temperature. After being rinsed 3 times with PBS, the samples were then blocked by goat serum and mouse monoclonal antihuman p-selectin antibody was added to each sample by using a same procedure of p-selectin quantity characterization. Subsequently, 30 μL of FITC-conjugated goat anti mouse IgG antibody was added to the samples and incubated at 37 °C for 30 min. After being rinsed 3 times with PBS, the samples were ultimately observed by fluorescence microscopy (Olympus IX51, Japan).

2.10.2. AT III Binding and APTT Assay. The development of anticoagulant activity of the residual heparin during the release were evaluated by antithrombin III (AT III) binding and activated partial thromboplastin time (APTT) assay. The amount of absorbed AT III on sample surfaces was determined semiquantitatively by immunochemistry as described previously.[25]

For APTT assay, 350 μL of PPP was first added to samples and incubated at 37 °C for 15 min. One hundred microliters of the incubated PPP was then transferred to the test tube and analyzed in an automatic blood coagulation analyzer (ACL-200, Beckman Coulter, USA) according to the test prescription.

2.10.3. FGN Adsorption and Conformation Change. Fibrinogen (FGN) adsorption and conformation change on different sample surfaces were evaluated to further determine the development of the anticoagulant activity during release. Both FGN adsorption and conformation change assay were detected using indirect immunochemistry using appropriate antibodies for total fibrinogen and FGN γ chain, respectively, as described elsewhere.[25]

2.11. Anti-inflammation Ability Evaluation. Macrophage cells seeding and TNF-α release assay were prepared to evaluate the alteration of anti-inflammation potential of NP-modified surfaces during release.

2.11.1. Macrophage Cell Isolation and Seeding. Macrophage cells were isolated from the peritoneum of Sprague−Dawley (SD) rat

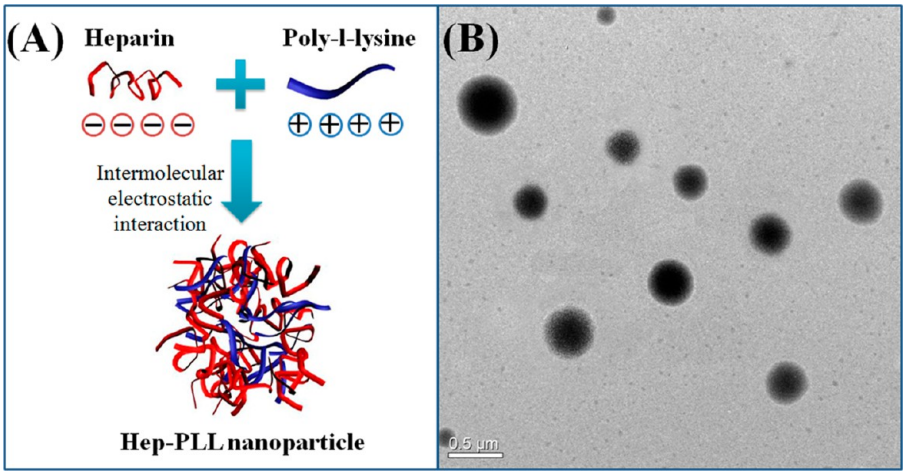

Figure 1. (A) Schematic drawing of Hep/PLL nanoparticle formation; (B) TEM images of prepared nanoparticle.

(Dashuo Co., Ltd., Chengdu) and cultured according to Li et al.[26] The cell density was adjusted to 1×10^5 cells/mL in DMEM for the experiments.

For macrophage cells seeding, 1 mL of cell suspension was added to the samples and incubated at 37 °C under 5% CO_2. Nonadherent cells were removed by washing with PBS after 2 h incubation, and 1 mL of fresh DMEM was then added to the samples for 24 h continuous incubation. Thereafter, the supernatant of each sample was collected for TNF-α and IL-6 assay. The samples were rinsed 3 times with PBS and fixed in 4% paraformaldehyde for 12 h at room temperature. Fifty microliters of rhodamine was then added to each sample surface and incubated at 37 °C for 30 min. After being rinsed 3 times with PBS, the samples were observed by fluorescence microscopy.

2.11.2. TNF-α and IL-6 Assay. Double-antibody sandwich ELISA was used to quantitative evaluate the tumor necrosis factor (TNF-α) and interleukin-6 (IL-6) content of collected supernatants. Briefly, 100 μL of each collected supernatant was added to a rabbit anti mouse TNF-α or IL-6 antibody-coated 96-well plate, and the test was set according to package insert directions of ELISA kit.

2.12. Cellular Compatibility Evaluation. In vitro EC and SMC performance on the samples was analyzed to investigate the antirestenosis potential and the potential for accelerated endothelium regeneration of the NP-modified surfaces at different stages during release.

2.12.1. EC and SMC Isolation and Culture. Endothelial cells (ECs) were isolated from human umbilical vein. Briefly, the lumen of umbilical vein was first thoroughly washed with physiological saline to remove the residual blood. Medium 199 (M199) containing 0.1% type II collagenase was then injected and incubated at 37 °C for 15 min. The digestion was stopped by filling M199 containing 10% FBS. Thereafter, the cell suspension were eluted and centrifuged at 1000 rpm for 8 min, the supernatant was subsequently removed and the precipitate of ECs were resuspended in M199 containing 15% FBS and 20 μg/mL endothelial cell growth supplement (ECGS) and incubated at 37 °C under 5% CO_2.

Smooth muscle cells (SMCs) were isolated from human umbilical artery. Briefly, adventitia layer and endothelium layer that surrounded umbilical artery were first stripped away and the residual tissue was cut into small pieces. Then, the artery pieces were cultured in Dulbecco's Modified Eagle Medium/F12 (DMEM/F12) containing 10% FBS at 37 °C under 5% CO_2. SMCs were obtained by outgrowth from these tissue pieces.

2.12.2. Cell Seeding on Sample Surfaces. All the samples were sterilized by ozone before cell seeding. ECs and SMCs were seeded on the samples at an identical density of 5×10^4 cells/cm^2 and incubated at 37 °C under 5% CO_2 for 1 day and 3 days.

2.12.3. Cell Proliferation Assay. The density and proliferation activity of different cells on different sample surfaces were investigated by manual cell counting and Cell Counting Kit-8 (CCK-8) assay, respectively. For CCK-8 assay, after 1 day and 3 days culture, the supernatant medium was removed and the samples were gently rinsed with PBS. Then 400 μL of fresh culture medium containing 10% CCK-8 reagent was added to the samples and incubated at 37 °C under 5% CO_2 for 3 h. The medium containing 10% CCK-8 was used as blank control. Subsequently, the absorbance was measured at 450 nm.

2.12.4. Immunofluorescence Staining. Immunofluorescence staining was preformed to indentify the types and observe the morphology of adherent cells on different sample surfaces. First, after 3 days culture, the samples were rinsed 3 times with PBS and then fixed in 4% paraformaldehyde for 12 h at room temperature. Thereafter, the samples were incubated with goat serum at 37 °C for 1 h to block the nonspecific adsorption. Thirty microliters of specific monoclonal rabbit IgG (first antibody) was added to sample surfaces and incubated at 37 °C for 30 min. After being rinsed 3 times with PBS, FITC-conjugated goat anti rabbit IgG antibody (second antibody) was added to samples and incubated at 37 °C for 30 min. The samples were subsequently thoroughly rinsed 3 times with PBS and observed by fluorescence microscopy. Here, the first antibody used for EC and SMC staining were rabbit monoclonal anti human vWF antibody and rabbit monoclonal anti human α-SMA antibody, respectively.

2.13. In Vivo Animal Experiment. In vivo experiment test was carried out by implanting the NP-modified samples into dog femoral arteries for 4 weeks. Ti was used as positive control. Two holes with a diameter of ~0.5 mm were predrilled at either end of 3×5 mm^2, double-sided polished and coated samples. The Ti- and dopamine-coated samples were first sterilized by autoclavation and the NP were prepared and immobilized under sterile conditions.

Three adult dogs (20−30 kg) were used in this experiment and each dog received four samples, two of each type. The samples were implanted and affixed to the inner surface of femoral artery by a medical suture passing through the sample hole. The dogs did not receive any anticoagulation after surgical. After implantation for 4 weeks, the samples were excised and rinsed by heparin solution to remove the residual blood, then observed immediately using a tridimensional microscope (Motic Images Plus 2.0 ML). Subsequently, the samples were fixed in 4% paraformaldehyde for 24 h at room temperature. After dehydration and critical point drying, the samples were observed by scanning electron microscopy.

2.14. Statistic Analysis. At least three independent experiments were performed for the tests described above. The data were analyzed with the software SPSS 11.5 and expressed as mean ± standard deviation (SD). The statistical significance between and within groups were determined by using two-way ANOVA in origin 8.0. The probability values $P < 0.05$ were considered significant difference ($^*P < 0.05$).

3. RESULTS

3.1. Morphology, Size, and Zeta Potential of Hep/PLL Nanoparticles. As shown in Figure 1A, in the neutral condition (PBS, pH 7.4), the highly negative charge density of heparin (Hep) contributed to its very strong electrostatic interaction with positively charged poly L-lysine (PLL), and led to the assembly of three-dimensional particle. TEM results (Figure 1B) further proved that the particles were successfully prepared and the particle size was in a nanoscale range.

Following ZETA-SIZER tests, the mean size of NP was 389 nm (Table 1). Particle dispersion index (PDI) is an important indicator to reflect the size distribution of particle suspension, and generally considered uniform when PDI value is less than 0.2. The determined values, listed in Table 1, indicate that the prepared NP presents favorable uniformity. The zeta potential of the NP suspension was above −30 mV (Table 1), promising sufficient stability of the formed nanoparticles.[22]

Table 1. Properties of Hep/PLL Nanoparticle

description	size (nm)	PDI	zeta potential (mV)
Hep-PLL nanoparticle	389 ± 51	0.12 ± 0.06	−31.3 ± 1.8

3.2. FTIR and XPS Result. The changes of surface chemical composition during release were determined by FTIR and XPS. Noticeable new peaks appeared in the FTIR spectra (Figure 2A) after NP immobilization compared to Ti-DM. A broad peak in the range from 3640 to 3370 cm^{-1} was considered as the overlap stretching vibrations peak of hydroxyl (−OH) and amine ($-NH_2$, −NH−) groups. The peak at 1600 cm^{-1} presents the vibration of the benzene ring framework of DM, and this peak shifted to 1640 cm^{-1} after NP immobilization, which may be contributed to the influence of amide I (C═O) bond stretching vibrations. A new small peak could also be observed at 1520 cm^{-1}, which corresponds to the stretching vibrations of the amide II (C−N, N−H) bond. The emergence of amine groups, amide I and II demonstrates the existence of PLL. Heparin is rich in carboxyl group (−COOH) and sulfonic group ($-SO_3$), and characteristic absorption peaks could also be observed at 1288, 1223, and 1042 cm^{-1}, which are ascribed to the C−O−S, S═O, and C−O−C bond, respectively. With the prolongation of release period, the intensity of those characteristic peaks gradually decreased, and it seems hard to distinguish the coated surfaces from the DM control after 28 days.

XPS analysis was used to further determine the elemental composition of sample surfaces. As shown in Figure 2B, new S 2s (∼234.6 eV) and S 2p (∼168.8 eV) peaks appeared in the spectrum after NP immobilization, and these peak could be observed even after 28 days, which indicates residual heparin on sample surfaces throughout the whole release process. The elemental content of the surface was calculated (Table 2). Obviously, the sulfur content presented a decreasing trend during release, and significantly dropped from 2.55% at 0 day to 1.02% at 28 day. Nitrogen showed an increasing tendency first (8.07% at 0 day to 10.87% at 10 day), then decreased again (10.87% at 10 day to 9.01% at 28 day). As described in 3.1, the surface of nanoparticles was mainly composed of heparin, and thereby with the continual release of heparin, the inner PLL may be exposed and cause the initial increase of the nitrogen content. Then, the PLL also elutes from the surface and the nitrogen content decreases again.

3.3. AFM images of nanoparticle morphology. The alteration of NP-modified surface topography was investigated by AFM.

As shown in Figure 3, the bare DM coating presented a quite smooth morphology. The particles on the NP immobilized surface were uniformly distributed with a mean size of ∼390 nm. During release, the particle maintained sphere morphology at day 1 but significantly changed and presented irregular degradation morphology at day 3 as sign of a rapid release of the biomolecules. Then, the particle size remain presented a rapid decreasing tendency from day 5 to day 10 (∼250 nm at day 5, ∼150 nm at day 7 and ∼100 nm at day 10), as well as the residual NP density. After that, no obvious changes of NP size could be observed from day 14 to day 28, but the NP density was slightly decreased, which may indicate that the biomolecules release behavior was tended to balance. After 28 days, there were still small amounts of NP left in the surfaces, which may contribute to the prevention of adverse cardiac events in the long term.

3.4. Quantitative Characterization Result of Heparin and Amine. The cumulative release amount of heparin and the residual density at each time point were quantified by TBO assay. Additionally, the change of the exposed amine density during release was determined by AO II assay.

Consistent with the AFM result, the NP immobilized surface initially presented a rapid heparin release behavior, the cumulative release amount of heparin at 10 day reached 7.8 ± 1.5 μg, and the residual heparin amount decreased from 12.2 ± 1.4 μg to 5.2 ± 0.6 μg (Figure 4A). Subsequently the heparin release curves tended to balance and there was still 3.8 ± 0.5 μg left on the surface after 28 days (Figure 4A). However, a different tendency was observed in amine density. The exposed amine density was continually increased from the initial 7.4 ± 0.5 nmol/cm^2 to 8.9 ± 0.6 nmol/cm^2 after 7 days, and then presented a slow downward trend and decreased to 7.1 ± 0.2 nmol/cm^2 at 28 day (Figure 4B). This result further confirms the assumption of AFM study and also confirms the observed trends of nitrogen content in the XPS result (Table 1).

3.5. Surface Hydrophilicity. Surface hydrophilicity is an important factor, which influences the amount of absorbed proteins, and subsequently the adhesion and fate of cells.[27] The hydrophilicity of solid materials surface was characterized by water contact angle analysis.

As shown in Figure 5, the water contact angle on Ti surface was 70.1 ± 4.5° and slightly decreased to 63.1 ± 4.3° on DM coated surface. The DM coating consists of numerous hydrophobic benzene rings and hydrophilic amine groups, phenolic hydroxyl group and benzoquinonyl, which have an integral effect on the surface hydrophilicity. Heparin and PLL are rich in hydrophilic groups, such as hydroxyl, amine, carboxyl and sulfo groups. Thereby, the water contact angle significantly decreased after NP immobilization (Figure 5). During release, the surface hydrophilic presented no significant changes from day 0 to day 5 and the contact angles remained between 20 and 30° (Figure 5). With ongoing release, however, the contact angle tended to increase and reached 44.5 ± 5.3° at day 28. It can be concluded that after 28 days, the Hep-PLL immobilized surface still exhibited better hydrophilicity than the only DM-coated surface.

3.6. Blood Compatibility Evaluation. *3.6.1. Platelet Adhesion and Activation.* P-selectin is a thrombo-inflammatory molecule involved in platelet activation and aggregation. Figure 6A shows the p-selectin staining of adhered platelet on

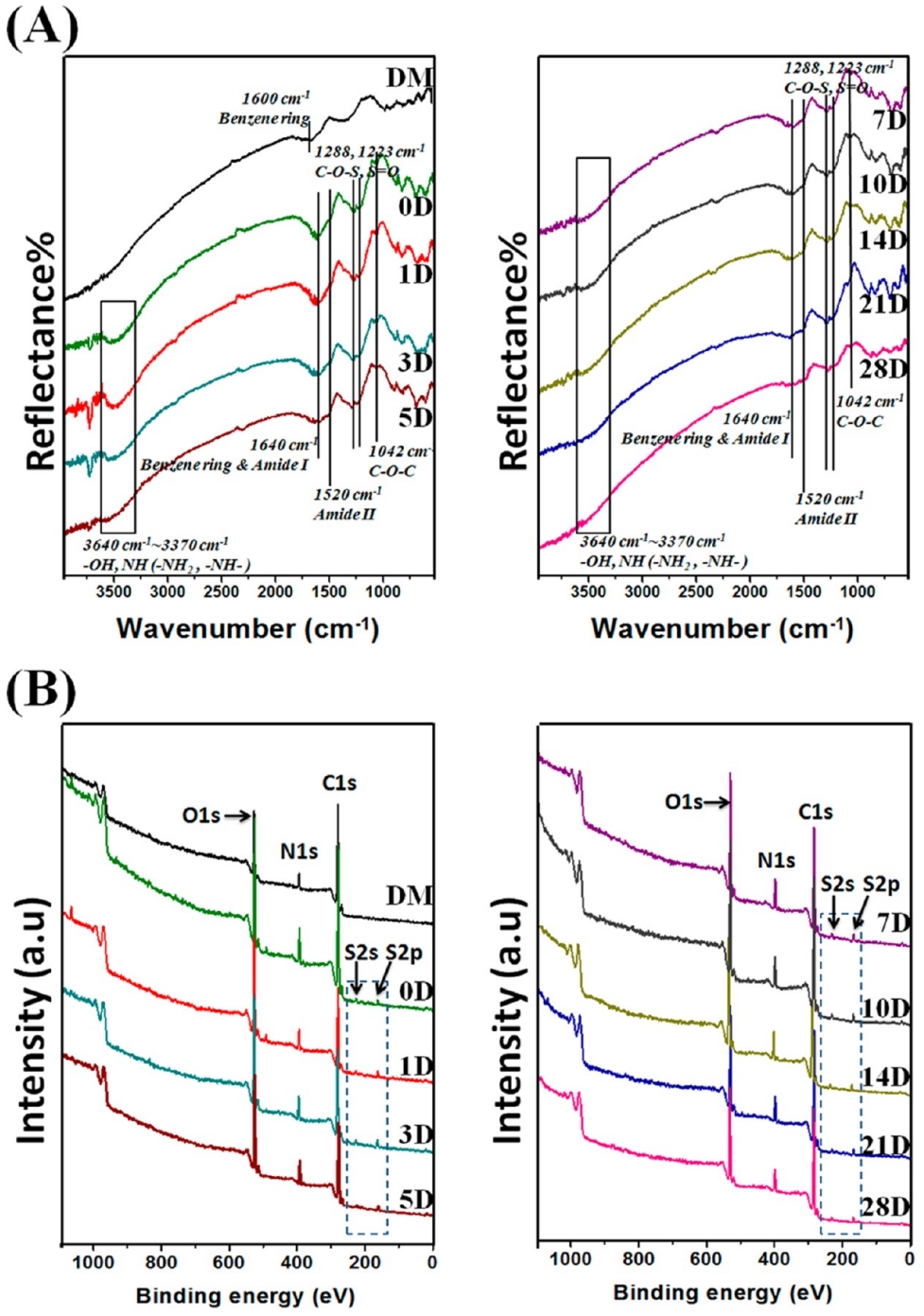

Figure 2. Surface chemical composition characterization. (A) FTIR spectra and (B) XPS wide-scan of NP-modified surfaces after dynamic release for different times. DM-coated Ti was used as blank control.

the samples. Obviously, platelets adherent on Ti- and DM-coated surface presented more prominent spreading and aggregation as signs of low hemocompatibility compared to the few platelets, exhibiting round shape on the NP-modified surface (0D). The density of adherent platelets on the sample surfaces gradually increased over the release period and presented evident spreading morphology on samples with release times over 14 days.

LDH from the cytoplasm of adherent blood platelets is released when the cells are lysed by the detergent Triton-X 100, and its amount is proportional to the cell number.[28] Consistent with the staining result, the relative amount of LDH (Figure 6B) and p-selectin (Figure 6C) greatly decreased on the NP-immobilized surface and presented no significant changes in the initial 10 days. Although the LDH release and p-selectin expression curve exhibiting an upward tendency when release period was above 14 days, the surface blood compatibility remains better than that of the Ti- and DM-coated surface even after 28 days.

3.6.2. AT III Binding and APTT Results. Activated partial thromboplastin time (APTT) is a common clinical coagulation test that is highly sensitive to heparin. According to Figure 7, the APTT value of platelet poor plasma (PPP) incubated with Ti or DM was in the normal range of blood clotting time (22–

dx.doi.org/10.1021/am5015309 | ACS Appl. Mater. Interfaces 2014, 6, 8729–8743

Table 2. Elemental Composition of Samples Surface during Dynamic Release Determined by XPS

release days	C (%)	N (%)	O (%)	S (%)
Ti-DM	75.41	6.80	17.79	0.00
0D	64.56	8.07	24.82	2.55
1D	64.16	8.82	24.90	2.12
3D	64.31	9.86	23.94	1.89
5D	64.61	10.32	23.27	1.80
7D	63.77	10.87	23.38	1.98
10D	67.25	8.41	22.46	1.88
14D	67.77	9.08	21.54	1.61
21D	66.86	9.03	22.71	1.40
28D	67.56	9.01	22.41	1.02

38 s), whereas the immobilization of NP completely suppressed coagulation (clotting time >189 s) (Figure 7). With the prolongation of release time, the APTT value gradually decreased and the tendency was consistent with the heparin residual amount curve (Figure 4A). After 28 days, although the mean APTT value of NP-modified surface was decreased to 45 s, approximately 14 s prolongation compared with Ti and DM (Figure 7), indicating that the samples still show anticoagulant properties.

AT III binding ability on sample surfaces was used to evaluate the development of the anticoagulant property during release. As shown in Figure 7, although a trace amount of AT III adsorbed on the Ti and DM surface, the anticoagulant activity however has no enhancement without the participation of heparin and thereby the APTT value was not prolonged. During release, the AT III binding curve exhibits a similar tendency as the curve of the residual heparin amount and further confirms the APTT result.

3.6.3. FGN Adsorption and Conformation Change. Fibrinogen (FGN) adsorption and subsequent conformation change on materials surface plays a critical role in platelet adhesion, aggregation and activation.

Compared with pure Ti and DM, the amount of adsorbed FGN was slightly decreased on NP immobilized surface, increased again and reached a constant level after 7 days (Figure 8). Although the negatively charged Hep/PLL nanoparticle should inhibit FGN adsorption in theory, protein adsorption on materials surface not only depends on the surface charge, but also determined by surface roughness, hydrophilicity, architecture, and chemical composition. The specific three-dimensional structure of NP and exposed dopamine coating may facilitate protein adsorption and thereby cause no significant decreasing of FGN adsorption on NP-modified surfaces during release compared to Ti (Figure 8). However, although the amount of adsorbed FGN was comparable, the biological conformation was very different on different sample surfaces. According to Figure 8, the FGN conformation change on the NP-immobilized surface was greatly decreased compared with Ti and DM ($*p < 0.05$), and also after 28 days dynamic release, the surface presented high efficiency to prevent FGN activation. The activation ratio calculated by dividing the mean value of FGN conformation change into FGN adsorption value further provides evidence that the NP-modified surface possesses powerful activity in preventing FGN conformation change.

3.7. Anti-inflammation Evaluation. The morphology and number of adherent macrophages on different sample surfaces, as well as the release of TNF-α and IL-6 after 24 h incubation, were detected and are given in Figure 9. The fluorescence images (Figure 9A) show that the macrophages extended pseudopods and presented irregular shape on the Ti and Ti-DM surfaces, whereas fewer pseudopods extended and the round shape appeared for macrophages on the NP-modified surface. The number of adherent macrophages on the NP-modified surface was significantly lower than that on Ti and Ti-DM surface ($*p < 0.05$), but it increased slightly during the release period. Interestingly, the pure DM coating could inhibit macrophages adhesion ($\#p < 0.05$), which was considered due to the immunomodulatory effects of dopamine on inflammation.[29] Once the macrophages adhere on a biomaterials surface, inflammatory cytokines are quickly produced and reach their peak concentrations within 24 h.[30] Therefore, a single incubation time of 24 h was selected in this study. As shown in Figure 9 , with the prolongation of release period, the amount of released TNF-α and IL-6 on the NP-modified surface slightly increased, but remained lower than that on Ti and Ti-DM surface after 28 days ($*p < 0.05$). In addition, the TNF-α and IL-6 level were normalized to the adherent cell number (Figure 9 B). The result further proved that the NP-modified surface could not only prevent macrophages adhesion and activation, but also reduced the release of inflammatory cytokines from the single cell.

3.8. Cytocompatibility Evaluation. ECs and SMCs were seeded on the sample surfaces to evaluate the development of cytocompatibility of the NP-modified surface during the release. Immunofluorescence staining was used to identify the cell types and detect the morphologies of adherent cells. Cell counting kit-8 (CCK-8) assay was performed to investigate the cell activity. The CCK-8 value at day 3 was normalized to the mean value at day 1 with the aim of calculating the proliferation rate of adherent cells.

As shown in Figure 10A1, the adherent cell density and activity were significantly decreased compared with Ti and Ti-DM (Figure 10 A2). With extended release time, however, the cell density, projected area, activity and proliferation rate gradually increased (Figure 10 A1 and A2). ECs grown on samples, which were eluted for more than 10 days showed higher metabolic activity and proliferation rate than Ti and Ti-DM ($*p < 0.05$). On the other hand, the metabolic activity and proliferation rate of adherent SMCs were also greatly decreased ($*p < 0.05$) on NP-modified surface compared with Ti and Ti-DM, and presented a slowly rising trend with the prolongation of the release period (Figure 10 B2). According to the SMCs immunofluorescence staining result (Figure 10 B1), the morphology of SMCs transformed from the normal spindle shape on Ti and Ti-DM surface, to an unhealthy round or irregular shape on the NP-modified surface, and returned to normal on samples with extended release period. Although the spreading area and metabolic activity of SMCs were significantly increased compared with 0D when the release time exceeded 14 days ($\#p < 0.05$), the CCK-8 value and proliferation rate were obviously lower than Ti and Ti-DM ($*p < 0.05$) (Figure 10 B2).

3.9. In Vivo Animal Test. In vivo animal tests were performed in dog femoral arteries to further evaluate the "time-ordered" potential of the NP-modified surface. To acquire the real biological response after material implantation, the dogs did not receive any anticoagulation after surgery. Figure 11 shows the typical optical microscope and SEM images of the control Ti and the NP-modified discs after 4 weeks implantation. Obviously there was severe thrombus formation

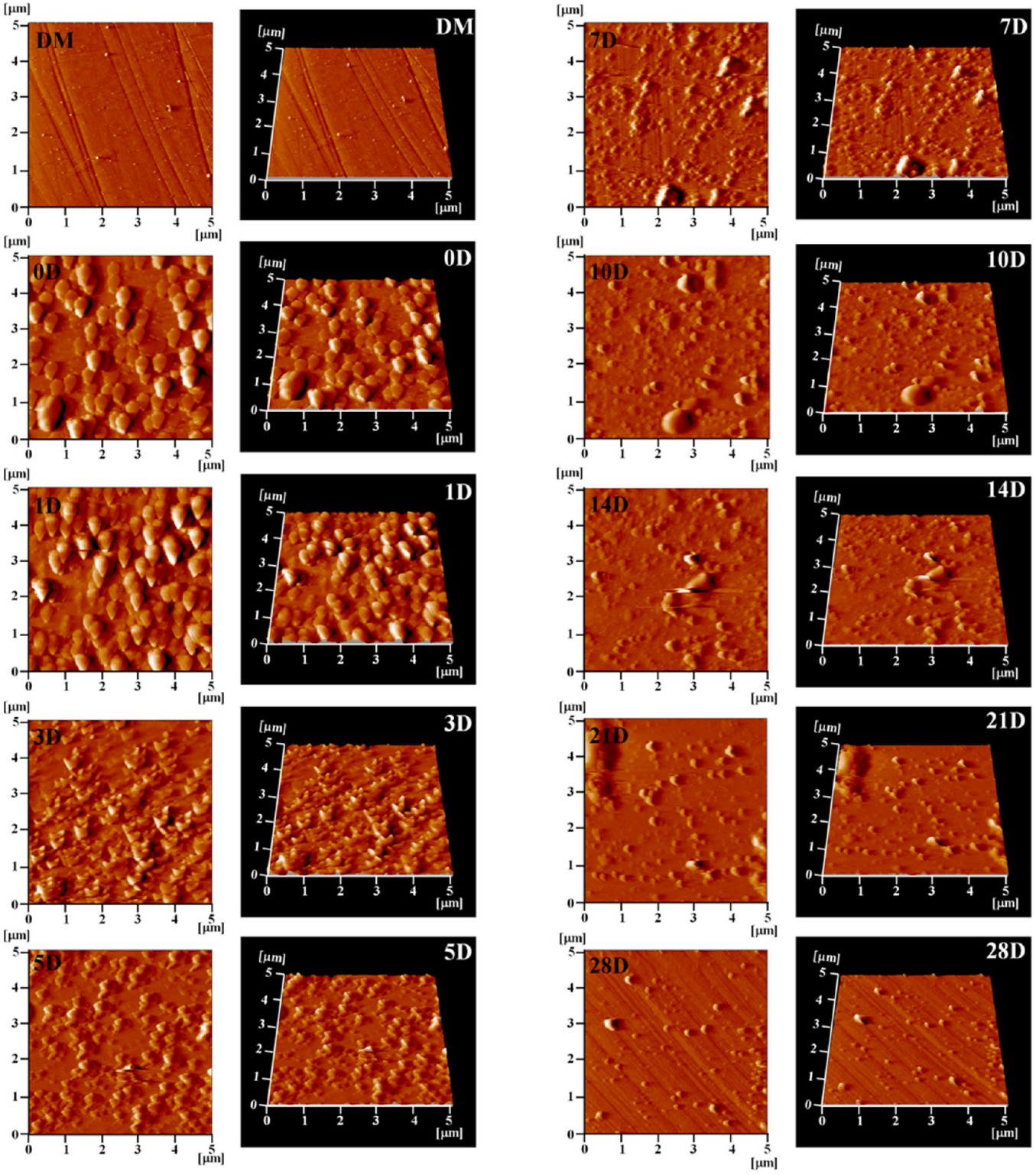

Figure 3. AFM morphology images of the alteration of NP-modified surface during dynamic release. DM coated Ti was used as blank control.

on Ti surface and even extended to the inner surface of blood vessel. In addition, a thick neo-intimal was formed on the Ti surface and the tissue around the rim of Ti disc presented long fusiform shape in the SEM images, which resembles smooth muscle tissue and indicates serious intimal hyperplasia and incomplete endothelialization (Figure 11). In contrast, the NP-modified surface presented no thrombus formation, and the thickness of neointimal tissue was significantly thinner than on the Ti surface. The NP-modified surface presented evenly covered by confluent endothelium in the SEM images, and it could be identified that tightly endothelium layer was formed and aligned in the direction of the blood flow. The in vivo results demonstrate that the NP-modified surface effectively inhibits thrombus formation and intimal hyperplasia, and it supports endothelium regeneration.

dx.doi.org/10.1021/am5015309 | ACS Appl. Mater. Interfaces 2014, 6, 8729−8743

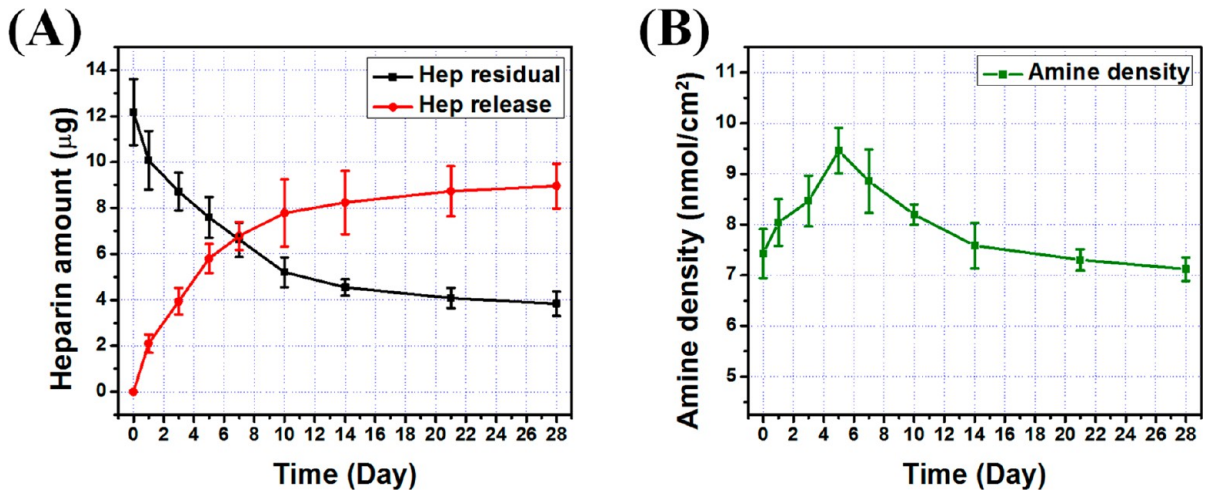

Figure 4. (A) Quantitative characterization of the cumulative release and residual amount of heparin at each time point during dynamic release (mean ± SD, N = 12); (B) exposed amine density during dynamic release (mean ± SD, N = 12).

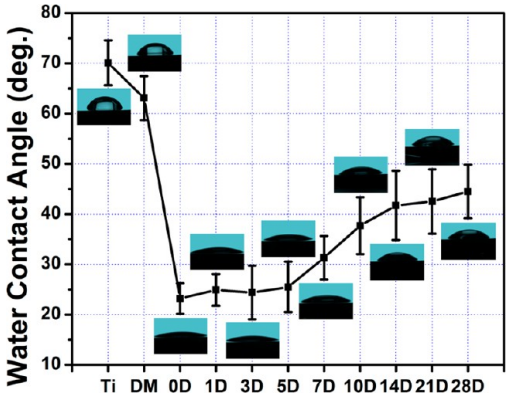

Figure 5. Alteration of surface water contact angle during the process of dynamic release (mean ± SD, N = 6).

4. DISCUSSION

The emergency of DES triggered a revolution in intervention cardiology. By the release of antiproliferative drugs from a stent surface, DES apply local pharmacotherapy to inhibit vascular SMC proliferation and thereby contribute to a reduction of 50−70% in the restenosis rate compared with bare metal stent (BMS).[31] However, late thrombosis and restenosis caused by delayed endothelialization continue to be the major constraint in clinical application. Nowadays, biofunctional surface modifications to prevent thrombosis formation, intimal hyperplasia, inflammation, as well as induce endothelium regeneration have been become a new hotspot. By specific biofunctional molecule screening, bioactivity promoting, optimized coating technologies, control of dosage and release behavior, and appropriate combination of surface chemistry and architecture, surface biofunctional modification techniques have made remarkable achievements. However, numerous surface modifications could provide favorable biocompatibility in vitro but exhibited dissatisfactory performance in vivo. Even for the clinically applied CD34 antibody-coated stent, higher rates of stent thrombosis and major adverse cardiac events were presented after 6 months compared to bare 316L SS stent.[32] The main reason for the difference between in vitro and in vivo results is seen in inadequate biocompatibility evaluation protocols. Insufficient knowledge about the biological processes in vivo and simplistic biocompatibility evaluation in vitro made it difficult to predict the pathologic processes at the implantation site in response to a foreign material. Thereby, it is important when designing a study that the physiological time course of the biological response to an implant material is considered appropriately.

As described above, the pathologic response after BMS implantation follows a defined sequence. Once the biomaterials come in contact with blood flow, plasma proteins including albumin, immunoglobulin and fibrinogen begin to adhere to the surface within milliseconds.[33] Then, platelets and other blood cells interact with the absorbed protein layer and adhere on the biomaterial surfaces. High levels of fibrinogen adsorption and conformation changes on the surface facilitate platelets adhesion and activation, and may cause acute thrombosis within minutes to hours. On the other side, endothelium injury caused by biomaterial implantation may trigger the activation of surrounding ECs. Those activated ECs and activated platelets release chemokines and proinflammatory factors to induce monocyte recruitment to the implantation site, leading to an inflammatory response.[34,35] The inflammatory reaction generally occurs within days to weeks, with a maximum at 1−2 days according to in vivo studies and clinical observations.[5,36] Inflammation accelerates platelets activation and subacute thrombus formation,[34] and stimulates excessive SMC proliferation and intimal hyperplasia.[5,37] Although numerous clinical follow-up studies show a peak of intimal hyperplasia at 3−6 months,[38,39] the rapid proliferation of SMCs induced by endothelium and inflammation shows its peak at 1−2 weeks and tends to balance after 4 weeks.[40,41] Excessive proliferation of SMCs at early stage is closely related to the occurrence of middle-to-late restenosis. Thereafter, incomplete endothelialization and insufficient biocompatibility of the exposed surface are major reasons for in-stent thrombosis and restenosis at middle stage (1−3 months). For BMS, the material is completely embedded in new born vascular tissue, and adverse tissue-material interface interaction may trigger negative remodeling of the neointima and cause the occurrence of late restenosis.

For new concepts of cardiovascular stent design, especially for biofunctional surface modification, the polymer coating is typically abolished and the exposed biomaterial surface will directly interact with the microenvironment in vivo. Thereby, it

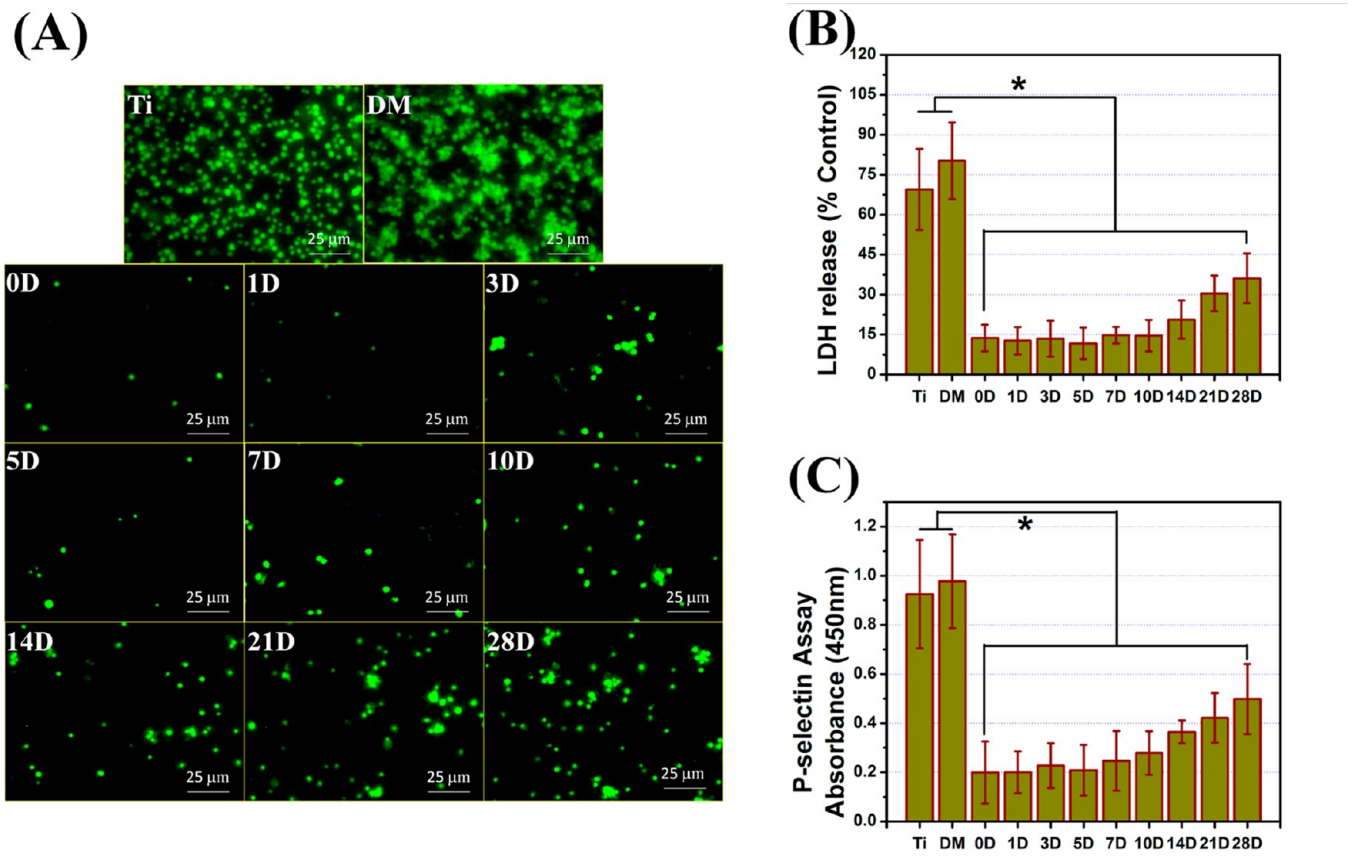

Figure 6. (A) P-selectin immunofluorescence staining of adhered platelets on different sample surfaces; (B) semiquantitative characterization of LDH release; (C) semiquantitative characterization of p-selectin expression. (mean ± SD, $N = 6$, $^*p < 0.05$ means significant difference in compared with Ti and Ti-DM).

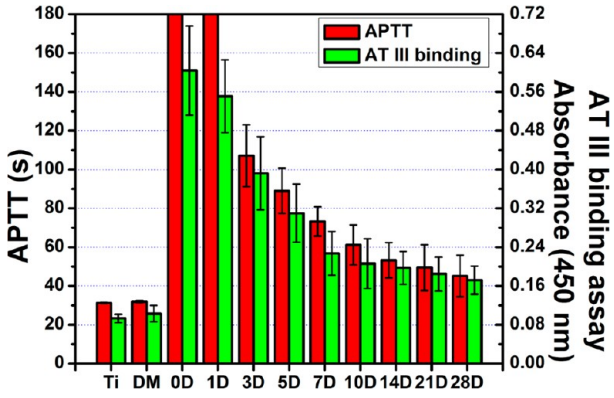

Figure 7. Alteration of AT III binding amount and clotting time of NP-modified surfaces during dynamic release. (mean ± SD, $N = 6$).

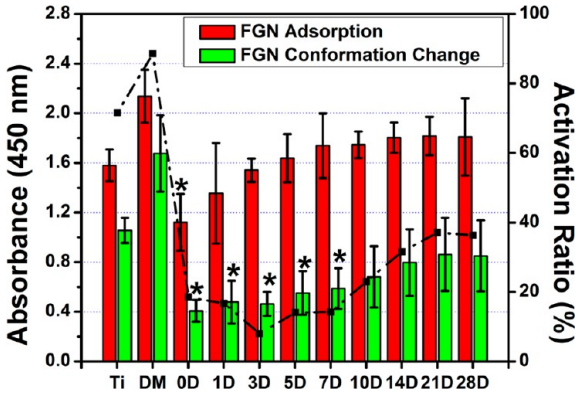

Figure 8. FGN adsorption and conformation change on different sample surfaces. The black dashed line refers to FGN activation ratio and calculated by dividing the mean absorbance value of FGN conformation change by that of adsorption. (mean ± SD, $N = 6$, $^*p < 0.05$ means significant difference in compared with Ti and Ti-DM).

is important for surface modification to take the time-ordered development of the implantation site of BMS into consideration and apply right remedy at the different stages. As we suggested, a reasonable biofunctional modification on cardiovascular material surfaces should first provide powerful effects in preventing the occurrence of thrombosis, inflammation, and SMC overproliferation for 2 weeks at least, and continue maintaining favorable hemocompatibility and anti intimal hyperplasia ability for another 2 weeks at least. On this basis, accelerate endothelialization as soon as possible and form a confluent endothelium layer within 1−3 months, with the aim of preventing the occurrence of thrombosis and restenosis at middle and late stage.

Ti and its alloys have been widely used in orthopedic, dental biomedical, and stent applications because of their excellent mechanical properties and biocompatibility. Recently, dopamine has attached much attention for its ability to form firmly adhesive interaction with almost all kinds of surfaces, in particular with metal surfaces by forming strong coordination bonds. Besides, dopamine coating has a specific reactivity for biomolecules containing sulfhydryl or amine groups and greatly facilitates the surface biofunctional modification of Ti.[42,43] However, although the dopamine coating has been reported

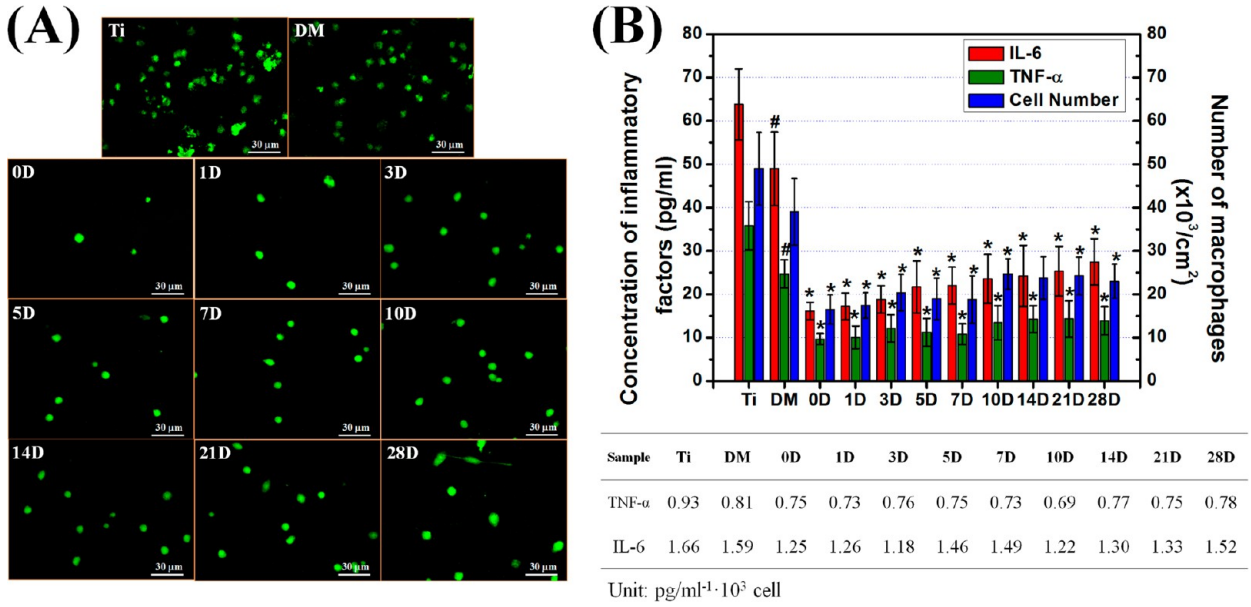

Sample	Ti	DM	0D	1D	3D	5D	7D	10D	14D	21D	28D
TNF-α	0.93	0.81	0.75	0.73	0.76	0.75	0.73	0.69	0.77	0.75	0.78
IL-6	1.66	1.59	1.25	1.26	1.18	1.46	1.49	1.22	1.30	1.33	1.52

Unit: pg/ml^{-1}·10^3 cell

Figure 9. (A) Rhodamine fluorescence staining of the morphology of adhered macrophages on different samples surface; (B) expression of TNF-α and IL-6 released by adhered macrophages after 24 h incubation, the date listed in the table were normalized to the mean value of adhered cell number. (mean ± SD, $N = 6$, $^*p < 0.05$ means significant difference in compared with Ti and Ti-DM, $^{\#}p < 0.05$ means significant difference in compared with Ti).

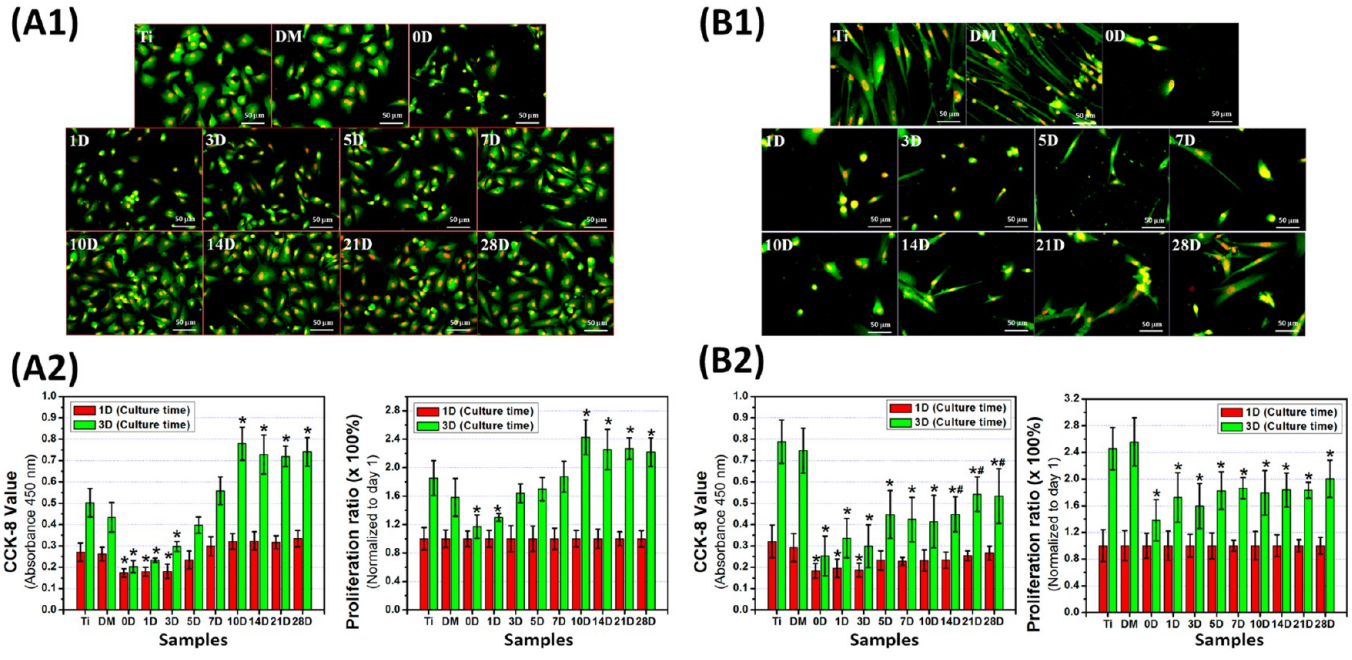

Figure 10. Immunofluorescence staining of specific cell surface antigens of (A1) vWF for ECs and (B1) α-actin for SMCs after 3 days culture, (A2, B2) CCK-8 value detected after 1 day and 3 days culture. The CCK-8 value at day 3 was normalized to day1 to calculate the proliferation ratio. (mean ± SD, $N = 6$, $^*p < 0.05$ means significant difference compared to Ti and Ti-DM, $^{\#}p < 0.05$ means significant difference compared to 0D).

has the ability to suppress excessive SMCs proliferation, poor blood compatibility strictly excluded the clinical application. In our previous study, a heparin gradient density was constructed on a dopamine coated surface by immobilizing Hep/PLL nanoparticles, with the aim of investigating the influence of heparin dosage on vascular cells behavior.[22] On this basis, a special type of Hep/PLL nanoparticle was selected and used for surface modification of dopamine-coated Ti. This type of particle processes favorable stability, sufficient binding density, and an adequate heparin release behavior, and is expected to meet the requirements of "time-order".

An in vitro dynamic release model that mimics in vivo blood flow condition was set up in this study to investigate the release behavior of heparin and PLL and the alteration of physicochemical surface properties, as well as the resulting changes of surface biocompatibility. The alterations of chemical surface composition and morphology were monitored by FTIR, XPS, and AFM. Successful immobilization of the NP on the dopamine surface was demonstrated. During of the release

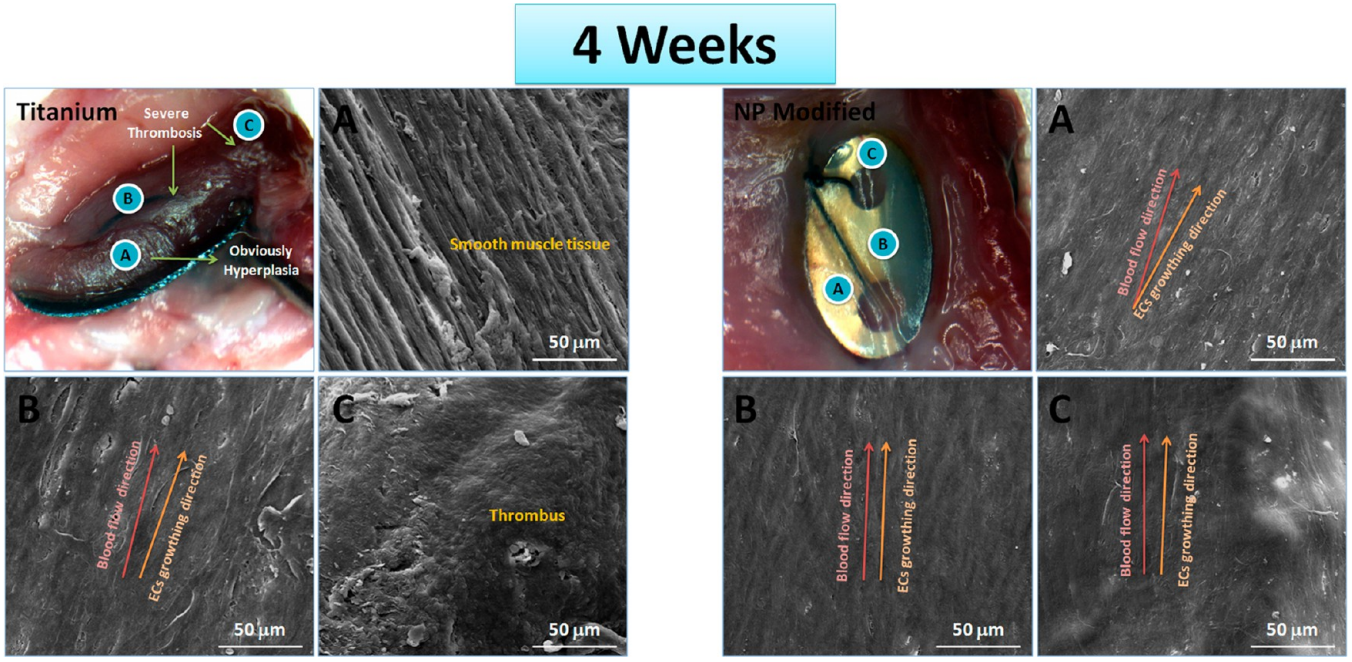

Figure 11. OM and SEM images of pristine Ti and NP-modified Ti implanted into femoral artery of dogs for 4 weeks. Left: (A, B) SEM morphology of the side edge tissue and the middle place tissue, respectively, and (C) thrombus morphology at the end of the sample; Right: (A–C) tissue morphology at the side edge, middle place, and the end of the samples, respectively.

period, the intensity of specific FTIR absorption peaks (Figure 2A) and the sulfur content (Table 2) gradually decreased. AFM images showed that the size and the density of immobilized NP were significantly decreased within 1–7 days, reaching a steady state in the following 3 weeks (Figure 3). XPS and AFM results demonstrated that there were still trace amounts of heparin left on the surface after 28 days. Consistent with these observations, the release behavior of heparin (Figure 4A) showed a rapid release within 7 days, which then tended to balance. The initial burst release of heparin is suggested necessary for preventing acute/subacute thrombosis and inflammation after the stent implantation.[44] The exposed amine density on the NP-modified surface during release was increased within the first 5 days, and then gradually decreased (Figure 4B). This was attributed to a preferential heparin exposure on the NP surface and exposure of internal PLL after the heparin burst release. However, with extended release period, PLL eluted from the surface, seen in a decreased amine density. According to our previous study, the amine density in this range does no harm to the cell growth.[22] The hydrophilicity of the NP-modified surface was significantly promoted, although the water contact angle gradually increased with the prolongation of release period, the surface remained hydrophilic (Figure 5).

The alteration of the surface chemistry, architecture, and hydrophilicity trigger quantitative and qualitative changes in the absorbed proteins, and affect the subsequent adhesion of blood platelets and behavior of blood vessel cells.[45] Thereby, assays for in vitro hemocompatibility, inflammatory reaction, and cytocompatibility were carried out, as well as in vivo animal tests to evaluate the time-ordered potential of the NP-modified surface during release. The blood compatibility of NP-modified surface correlated positively with the residual heparin density. The burst release of heparin can prevent acute thrombosis at the initial stage, but AT III binding and APTT results (Figure 7) demonstrated that the surface anticoagulation potency of NP-modified surface significantly decreased within this burst release phase (1–7 days). Also, fibrinogen absorption tests indicated a low activation ratio of the absorbed fibrinogen on the surfaces during the 1 to 7 days (Figure 8), and platelet adhesion and activation results (Figure 6) further demonstrated that the NP-modified surface was competent to provide excellent blood compatibility within 7 days. After the 7 days release period, however, the fibrinogen activation rate increased (Figure 8) and the adherent platelets were partially activated (Figure 6A). However, LDH release and p-selectin expression show that number and activation level of adherent platelets on the NP-modified surface also after 28 days remained significantly lower than on control Ti and Ti-DM (Figure 6B, C). Thus, the NP-modified surface meets the requirements of blood compatibility in the time-ordered process.

Inflammation in response to EC and platelet activation plays a critical role in the occurrence of subacute thrombosis and intimal hyperplasia. As a widely used anticoagulant, heparin also exhibits favorable anti-inflammatory effects in clinical therapy.[46] In this study, the time-ordered anti-inflammatory potential of NP was evaluated by investigating the influence of release period on the macrophage behavior. TNF-α and IL-6 synthesized by adherent macrophages are two important mediators in the inflammatory response. The NP-modified surface strongly inhibited macrophage adhesion and activation (Figure 9A). With the prolongation of release period, the number of adhered macrophages increased (Figure 9B), but they did not show signs of activation. TNF-α and IL-6 release further demonstrated that the residual heparin on NP-modified surface also after 28 days elution was sufficient to suppress inflammation (Figure 9B). By inhibit platelets activation, the NP-modified surface was expected to provide a more efficient effect in preventing the recruitment and activation of macrophages.[35] Besides, the clinically applied immunomodulator dopamine was found to suppress inflammation also in the form of a surface coating (Figure 9),[29] so the exposed free dopamine coating during the heparin release provides an

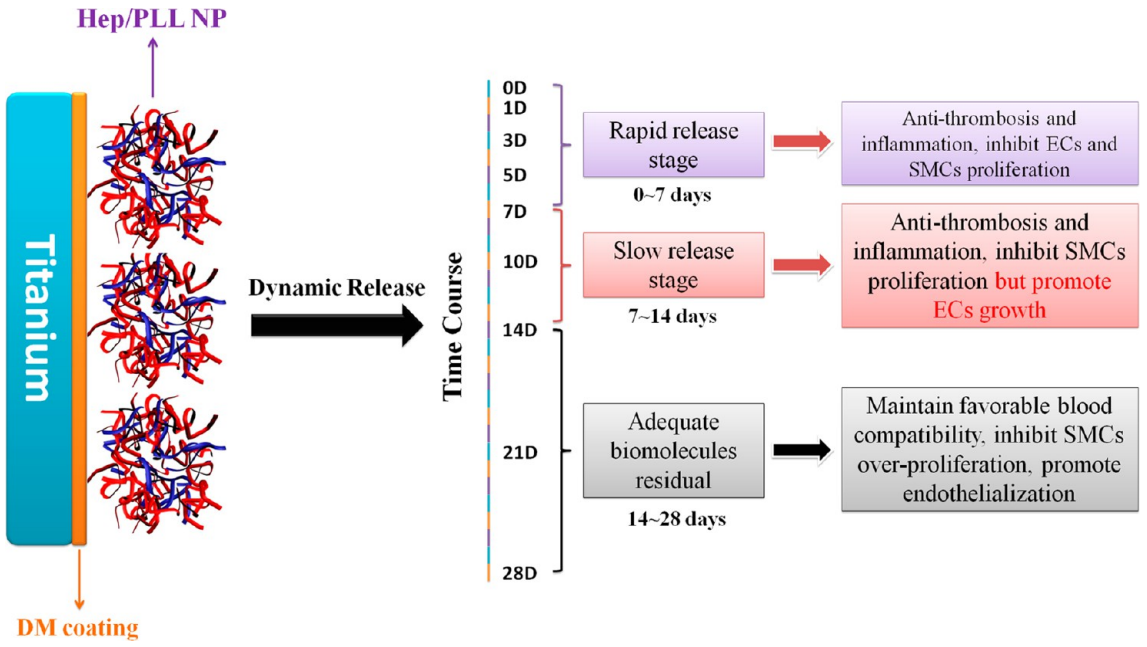

Figure 12. Stage-adjusted therapy potential of NP-modified surface to the intravascular biological response during dynamic release.

additional anti-inflammatory effect. In all, the NP-modified surface meets the required anti-inflammatory properties in the time-ordered process of stent healing.

Similar to the antiproliferative drugs, which are commonly used in current drug-eluting stents, heparin also possesses favorable antirestenosis properties and has been adopted as surface coating of cardiovascular stent for clinical use.[47,48] Numerous studies have shown that heparin is readily bound and internalized by ECs and SMCs.[49,50] Through electrostatic interaction with positively charged proteins, internalized heparin blocks some important intracellular signaling pathways, such as p38 mitogen-activated protein kinase (MAPK)- and nuclear factor-κB (NF-κB)-mediated intracellular transcription pathway,[51,52] PI3K/Akt-mediated cell proliferation and cytochrome c-mediated cell respiration,[53,54] and thereby inhibit cell adhesion, migration, and proliferation behaviors. In addition, the high negatively charged characteristic of heparin and heparinized surfaces prevent cell adhesion and proliferation. Therefore, although the heparin-modified surface can inhibit excessive SMCs proliferation, it may also delay endothelialization. According to our previous study, a heparin density on a biomaterial surfaces in the range of 3−7 μg/cm^2 selectively inhibits SMCs proliferation but promotes EC proliferation.[22] This phenomenon has been attributed to the specific interaction between heparin and growth factors such as VEGF, stromal cell derived factor-1α (SDF-1α and various extracellular cell matrix (ECM) proteins, which stimulate EC growth. The binding of these cytokines and proteins to heparin enhances their bioactivity and extends their half-life,[55] this behavior endows heparin with endothelialization stimulating properties. In this study, the proliferation and spreading of ECs and SMCs on NP-modified surface were significantly reduced due to the high heparin density (Figure 10). However, the proliferation metabolic activity of ECs and on the NP-modified surface rapidly improved with the prolongation of release period. For SMCs, although the proliferation activity was gradually increased during release, the growth was still significantly inhibited ($P < 0.05$) on the NP-modified surface after 28 days, compared with Ti or Ti-DM. On the whole, the NP-modified surface presents negative effects on ECs and SMCs growth in an early phase, but selectively accelerates ECs growth and inhibits SMCs proliferation after 10 days.

In vivo animal tests showed serious thrombus formation and intimal hyperplasia on the Ti surface after 4 weeks implantation (Figure 11). In contrast, the NP-modified surface showed no thrombus formation, but it was covered with confluent and flat endothelium, and thinner neointimal tissue than the control (Figure 11). This result further demonstrates that the dopamine-coated Ti surface modified by Hep/PLL nanoparticles was competent to provide a time-adjusted response to the pathological processes at the vessel wall after manipulation (Figure 12). Although the surface biocompatibility should be further evaluated through long-term in vivo experiments, the good performance in the early phase is a prerequisite to prevent adverse cardiac events in the middle and late phases. For the biofunctional surface modification of cardiovascular stents, because of the limitation of technology and biomaterial itself, it is hard to make the constructed functional layer to long-term direct the whole body biological response. The meaning of time-ordered surface modification is providing the time-adjusted remedy and guidance for the intravascular biological response after biomaterial implantation, and keeping the blood coagulation, inflammation reaction, and tissue regeneration in the normal range. On this basis, accelerated in situ endothelialization by induced stem/progenitor cell mobilization and differentiation will be studied as a next step.

5. CONCLUSION

A novel concept of time-ordered surface biofunctional modification has been introduced in the present work. On the basis of our previous study, we immobilized heparin/poly-L-lysine nanoparticles on a dopamine-coated surface and set up an in vitro dynamic release model to mimic in vivo blood fluid condition. With the prolongation of the release period, the physicochemical surface properties and biocompatibility was changed correspondingly. In conclusion, the NP-modified

surface possesses excellent properties against thrombosis, inflammation, and SMC proliferation within the first 7 days, but also suppresses ECs proliferation during this time. After 7 days, the NP-modified surface was able to selectively inhibit excessive SMCs proliferation and at the same time promote ECs growth. Up to the end of the analysis time of 28 days, the modified surface presented favorable blood compatibility and anti-inflammatory effect, as well as prevent intimal hyperplasia. This work provides a potential application in the surface modification of cardiovascular stent for time-adjusted intravascular biological response.

AUTHOR INFORMATION

Corresponding Author

*E-mail: chenjy@263.net.

Notes

The authors declare no competing financial interest.

ACKNOWLEDGMENTS

The authors gratefully acknowledge the assistance from Prof. Yuancong Zhao, and the financial support of Key Basic Research Program (2011CB606204), National Natural Science Foundation of China (31170916#, No. 31270020#), and the Fundamental Research Funds for the Central Universities (SWJTU11ZT11).

REFERENCES

(1) Boudriot, E.; Thiele, H.; Walther, T.; Liebetrau, C.; Boeckstegers, P.; Pohl, T.; Reichart, B.; Mudra, H.; Beier, F.; Gansera, B.; Neumann, F. J.; Gick, M.; Zietak, T.; Desch, S.; Schuler, G.; Mohr, F. W. Randomized Comparison of Percutaneous Coronary Intervention With Sirolimus-Eluting Stents Versus Coronary Artery Bypass Grafting in Unprotected Left Main Stem Stenosis. *J. Am. Coll. Cardiol.* **2011**, *57*, 538−545.

(2) Park, D. W.; Kim, Y. H.; Yun, S. C.; Lee, J. Y.; Kim, W. J.; Kang, S. J.; Lee, S. W.; Lee, C. W.; Kim, J. J.; Choo, S. J.; Chun, C. H.; Lee, J. W.; Park, S. W.; Park, S. J. Long-Term Outcomes After Stenting Versus Coronary Artery Bypass Grafting for Unprotected Left Main Coronary Artery Disease. *J. Am. Coll. Cardiol.* **2010**, *56*, 1366−1375.

(3) Mak, K. H.; Belli, G.; Ellis, S. G.; Moliterno, D. J. Subacute Stent Thrombosis: Evolving Issues and Current Concepts. *J. Am. Coll. Cardiol.* **1996**, *27*, 494−503.

(4) Haude, M.; Erbel, R.; Issa, H.; Straub, U.; Rupprecht, H. J.; Treese, N.; Meyer, J. Subacute Thrombotic Complications after Intracoronary Implantation of Palmaz-Schatz Stents. *Am. Heart. J.* **1993**, *126*, 15−22.

(5) Welt, F. G.; Rogers, C. Inflammation and Restenosis in the Stent Era. *Arterioscler. Thromb. Vasc. Biol.* **2002**, *22*, 1769−1776.

(6) Kornowski, R.; Hong, M. K.; Tio, F. O.; Bramwell, O.; Wu, H.; Leon, M. B. In-Stent Restenosis: Contributions of Inflammatory Responses and Arterial Injury to Neointimal Hyperplasia. *J. Am. Coll. Cardiol.* **1998**, *31*, 224−230.

(7) Geary, R. L.; Williams, J. K.; Golden, D.; Brown, D. G.; Benjamin, M. E.; Adams, M. R. Time Course of Cellular Proliferation, Intimal Hyperplasia, and Remodeling Following Angioplasty in Monkeys with Established Atherosclerosis. A Nonhuman Primate Model of Restenosis. *Arterioscler. Thromb. Vasc. Biol.* **1996**, *16*, 34−43.

(8) Chen, C.; Hughes, J. D.; Mattar, S. G.; Ku, D. N.; Lumsden, A. B. Time-Course Study of Intimal Hyperplasia in the Endarterectomized Canine Artery. *J. Surg. Res.* **1997**, *67*, 106−112.

(9) Miyazaki, K.; Nishibe, T.; Watanabe, S.; Kudo, F.; Katoh, H.; Yasuda, K.; Tanabe, T. Biological Response to Expandable Metallic Stents Implanted into the Portal Vein. A Histomorphometric Study. *J. Cardiovasc. Surg. (Torino)* **2000**, *41*, 885−890.

(10) Windecker, S.; Serruys, P. W.; Wandel, S.; Buszman, P.; Trznadel, S.; Linke, A.; Lenk, K.; Ischinger, T.; Klauss, V.; Eberli, F.; Corti, R.; Wijns, W.; Morice, M. C.; di Mario, C.; Davies, S.; van Geuns, R. J.; Eerdmans, P.; van Es, G. A.; Meier, B.; Jüni, P. Biolimus-Eluting Stent with Biodegradable Polymer Versus Sirolimus-Eluting Stent with Durable Polymer for Coronary Revascularisation (LEADERS): A Randomised Non-Inferiority Trial. *Lancet* **2008**, *372*, 1163−1173.

(11) Verheye, S.; Agostoni, P.; Dawkins, K. D.; Dens, J.; Rutsch, W.; Carrie, D.; Schofer, J.; Lotan, C.; Dubois, C. L.; Cohen, S. A.; Fitzgerald, P. J.; Lansky, A. J. The GENESIS (Randomized, Multicenter Study of the Pimecrolimus -Eluting and Pimecrolimus/Paclitaxel-Eluting Coronary Stent System in Patients with De Novo Lesions of the Native Coronary Arteries) trial. *JACC Cardiovasc. Interv.* **2009**, *2*, 205−214.

(12) Lansky, A. J.; Costa, R. A.; Mintz, G. S.; Tsuchiya, Y.; Midei, M.; Cox, D. A.; O'Shaughnessy, C.; Applegate, R. A.; Cannon, L. A.; Mooney, M.; Farah, A.; Tannenbaum, M. A.; Yakubov, S.; Kereiakes, D. J.; Wong, S. C.; Kaplan, B.; Cristea, E.; Stone, G. W.; Leon, M. B.; Knopf, W. D.; O'Neill, W. W. Non-Polymer-Based Paclitaxel-Coated Coronary Stents for the Treatment of Patients with De Novo Coronary Lesions: Angiographic Follow-Up of the DELIVER Clinical Trial. *Circulation* **2004**, *109*, 1948−1954.

(13) Adriaenssens, T.; Mehilli, J.; Wessely, R.; Ndrepepa, G.; Seyfarth, M.; Wieczorek, A.; Blaich, B.; Iijima, R.; Pache, J.; Kastrati, A.; Schömig, A. Does Addition of Estradiol Improve the Efficacy of A Rapamycin-Eluting Stent? Results of the ISAR-PEACE Randomized Trial. *J. Am. Coll. Cardiol.* **2007**, *49*, 1265−1271.

(14) Byrne, R. A.; Mehilli, J.; Iijima, R.; Schulz, S.; Pache, J.; Seyfarth, M.; Schömig, A.; Kastrati, A. A Polymer-Free Dual Drug-Eluting Stent in Patients with Coronary Artery Disease: A Randomized Trial vs. Polymer-Based Drug-Eluting Stents. *Eur. Heart. J.* **2009**, *30*, 923−931.

(15) Byrne, R. A.; Kastrati, A.; Tiroch, K.; Schulz, S.; Pache, J.; Pinieck, S.; Massberg, S.; Seyfarth, M.; Laugwitz, K. L.; Birkmeier, K. A.; Schömig, A.; Mehilli, J. 2-Year Clinical and Angiographic Outcomes from A Randomized Trial of Polymer-Free Dual Drug-Eluting Stents Versus Polymer-Based Cypher and Endeavor [Corrected] Drug-Eluting Stents. *J. Am. Coll. Cardiol.* **2010**, *55*, 2536−2543.

(16) Cindhuchao, N.; Quinn, D. A.; Garg, H. G.; Hales, C. A. Heparin Inhibits SMC Growth in the Presence of Human and Fetal Bovine Serum. *Biochem. Biophys. Res. Commun.* **2003**, *302*, 84−88.

(17) Hoshi, R. A.; Van Lith, R.; Jen, M. C.; Allen, J. B.; Lapidos, K. A.; Ameer, G. The Blood and Vascular Cell Compatibility of Heparin-Modified ePTFE Vascular Grafts. *Biomaterials* **2013**, *34*, 30−41.

(18) Guyton, J. R.; Rosenberg, R. D.; Clowes, A. W.; Karnovsky, M. J. Inhibition of Rat Arterial Smooth Muscle Cell Proliferation by Heparin. In Vivo Studies with Anticoagulant and Nonanticoagulant Heparin. *Circ. Res.* **1980**, *46*, 625−634.

(19) Jaster, M.; Schwimmbeck, P.; Spencker, S.; Schultheiss, H. P.; Rauch, U. Randomized Comparison of Platelet-Leukocyte Aggregates and Platelet Activation in Blood: Heparin-Coated Coiled Wire Stent Implantation Versus Balloon Angioplasty in Acute Myocardial Infarction. *Thromb. Res.* **2003**, *112*, 285−289.

(20) Lin, P. H.; Chronos, N. A.; Marijianowski, M. M.; Chen, C.; Bush, R. L.; Conklin, B.; Lumsden, A. B.; Hanson, S. R. Heparin-Coated Balloon-Expandable Stent Reduces Intimal Hyperplasia in the Iliac Artery in Baboons. *J. Vasc. Interv. Radiol.* **2003**, *14*, 603−611.

(21) Atalar, E.; Haznedaroğlu, I.; Aytemir, K.; Aksöyek, S.; Ovünç, K.; Oto, A.; Ozmen, F. Effects of Stent Coating on Platelets and Endothelial Cells After Intracoronary Stent Implantation. *Clin. Cardiol.* **2001**, *24*, 159−164.

(22) Liu, T.; Liu, Y.; Chen, Y.; Liu, S.; Maitz, M. F.; Wang, X.; Zhang, K.; Wang, J.; Wang, Y.; Chen, J.; Huang, N. Immobilization of Heparin/Poly-l-Lysine Nanoparticles on Dopamine Coated Surface to Create A Heparin Density Gradient for Selective Direction of Platelet and Vascular Cells Behavior. *Acta. Biomater.* **2014**, *10*, 1940−1954.

(23) Smith, P. K.; Mallia, A. K.; Hermanson, G. T. Colorimetric Method for the Assay of Heparin Content in Immobilized Heparin Preparations. *Anal. Biochem.* **1980**, *109*, 466−473.

(24) Hamerli, P.; Weigel, T.; Groth, T.; Paul, D. Surface Properties of and Cell Adhesion onto Allylamine−Plasma-Coated Polyethylenterephtalat Membranes. *Biomaterials* **2003**, *24*, 3989−3999.
(25) Li, G. C.; Yang, P.; Qin, W.; Maitz, M. F.; Zhou, S.; Huang, N. The Effect of Coimmobilizing Heparin and Fibronectin on Titanium on Hemocompatibility and Endothelialization. *Biomaterials* **2011**, *32*, 4691−4703.
(26) Li, G. C.; Yang, P.; Guo, X.; Huang, N.; Shen, R. An In Vitro Evaluation of Inflammation Response of Titanium Functionalized With Heparin/Fibronectin Complex. *Cytokine* **2011**, *56*, 208−217.
(27) Monchaux, E.; Vermette, P. Effects of Surface Properties and Bioactivation of Biomaterials on Endothelial Cells. *Front. Biosci. (Schol. Ed.)* **2010**, *2*, 239−255.
(28) Grunkemeier, J. M.; Tsai, W. B.; Horbett, T. A. Hemocompatibility of Treated Polystyrene Substrates: Contact Activation, Platelet Adhesion, and Procoagulant Activity of Adherent Platelets. *J. Biomed. Mater. Res.* **1998**, *41*, 657−670.
(29) Beck, G. C.; Brinkkoetter, P.; Hanusch, C.; Schulte, J.; van Ackern, K.; van der Woude, F. J.; Yard, B. A. Clinical Review: Immunomodulatory Effects of Dopamine in General Inflammation. *Crit. Care.* **2004**, *8*, 485−491.
(30) Cardona, M. A.; Simmons, R. L.; Kaplan, S. S. TNF and IL-1 Generation by Human Monocytes in Response to Biomaterials. *J. Biomed. Mater. Res.* **1996**, *26*, 851−859.
(31) Windecker, S.; Meier, B. Late Coronary Stent Thrombosis. *Circulation* **2007**, *116*, 1952−1965.
(32) Červinka, P.; Bystroň, M.; Špaček, R.; Kvašňák, M.; Jakabčin, J. Randomized Comparison of Genous Stent Versus Chromium-Cobalt stent for Treatment of ST-Elevation Myocardial Infarction. 6-month Clinical, Angiographic and IVUS Follow-up. GENIUS-STEMI trial. Presented at the American College of Cardiology Annual Scientific Session, 2009.
(33) Puleo, D. A.; Bizios, R. In *Biological Interactions on Materials Surfaces*; Schmidt, D. R., Heather, W., Weiyuan, J. K, Eds.; Springer: New York, 2009; Chapter 1, pp 1−18.
(34) Libby, P.; Simon, D. I. Inflammation and Thrombosis: the Clot Thickens. *Circulation* **2001**, *103*, 1718−1720.
(35) Wagner, D. D.; Burger, P. C. Platelets in Inflammation and Thrombosis. *Arterioscler. Thromb. Vasc. Biol.* **2003**, *23*, 2131−2137.
(36) Li, J. J.; Fang, C. H.; Jiang, H.; Huang, C. X.; Hui, R. T.; Chen, M. Z. Time Course of Inflammatory Response After Renal Artery Stenting in Patients with Atherosclerotic Renal Stenosis. *Clin. Chim. Acta* **2004**, *350*, 115−121.
(37) Li, J. J.; Nie, S. P.; Zhang, C. Y.; Gao, Z.; Zheng, X.; Guo, Y. L. Is Inflammation a Contributor for Coronary Stent Restenosis? *Med. Hypotheses* **2007**, *68*, 945−951.
(38) Kastrati, A.; Schömig, A.; Dietz, R.; Neumann, F. J.; Richardt, G. Time Course of Restenosis During the First Year after Emergency Coronary Stenting. *Circulation* **1993**, *87*, 1498−1505.
(39) Tamai, H.; Berger, P. B.; Tsuchikane, E.; Suzuki, T.; Nishikawa, H.; Aizawa, T.; Fujii, K.; Nozaki, Y.; Kyo, E.; Kobayashi, T.; Reiber, J.; Van Weert, A. W. Frequency and Time Course of Reocclusion and Restenosis in Coronary Artery Occlusions after Balloon Angioplasty Versus Wiktor Stent Implantation: Results from the Mayo-Japan Investigation for Chronic Total Occlusion (MAJIC) Trial. *Am. Heart. J.* **2004**, *147*, E9.
(40) Hanke, H.; Strohschneider, T.; Oberhoff, M.; Betz, E.; Karsch, K. R. Time Course of Smooth Muscle Cell Proliferation in the Intima and Media of Arteries Following Experimental Angioplasty. *Circ. Res.* **1990**, *67*, 651−659.
(41) Geary, R. L.; Kohler, T. R.; Vergel, S.; Kirkman, T. R.; Clowes, A. W. Time Course of Flow-Induced Smooth Muscle Cell Proliferation and Intimal Thickening in Endothelialized Baboon Vascular Grafts. *Circ. Res.* **1994**, *74*, 14−23.
(42) Weng, Y.; Song, Q.; Zhou, Y.; Zhang, L.; Wang, J.; Chen, J.; Leng, Y.; Li, S.; Huang, N. Immobilization of Selenocystamine on TiO2 Surfaces for in Situ Catalytic Generation of Nitric Oxide and Potential Application in Intravascular Stents. *Biomaterials* **2011**, *32*, 1253−1263.
(43) Lee, H.; Rho, J.; Messersmith, P. B. Facile Conjugation of Biomolecules onto Surfaces via Mussel Adhesive Protein Inspired Coatings. *Adv. Mater.* **2009**, *21*, 431−434.
(44) Lakshmi, T. S.; Shanmugasundaram, N.; Shanmuganathan, S.; Karthikeyan, K.; Meenakshi, J.; Babu, M. Controlled Release of 2, 3 Desulfated Heparin Exerts its Anti-Inflammatory Activity by Effectively Inhibiting E-Selectin. *J. Biomed. Mater. Res., Part A* **2010**, *95*, 118−128.
(45) Liu, T.; Liu, S.; Zhang, K.; Chen, J.; Huang, N. Endothelialization of Implanted Cardiovascular Biomaterial Surfaces: The Development from in Vitro to in Vivo. *J. Biomed. Mater. Res., Part A* **2013**, DOI: 10.1002/jbm.a.35025.
(46) Young, E. The Anti-Inflammatory Effects of Heparin and Related Compounds. *Thromb. Res.* **2008**, *122*, 743−752.
(47) Ahn, Y. K.; Jeong, M. H.; Kim, J. W.; Kim, S. H.; Cho, J. H.; Cho, J. G.; Park, C. S.; Juhng, S. W.; Park, J. C.; Kang, J. C. Preventive Effects of the Heparin-Coated Stent on Restenosis in the Porcine Model. *Catheter. Cardiovasc. Interv.* **1999**, *48*, 324−330.
(48) Serruys, P. W.; van Hout, B.; Bonnier, H.; Legrand, V.; Garcia, E.; Macaya, C.; Sousa, E.; van der Giessen, W.; Colombo, A.; Seabra-Gomes, R.; Kiemeneij, F.; Ruygrok, P.; Ormiston, J.; Emanuelsson, H.; Fajadet, J.; Haude, M.; Klugmann, S.; Morel, M. A. Randomised Comparison of Implantation of Heparin-Coated Stents with Balloon Angioplasty in Selected Patients with Coronary Artery Disease (Benestent II). *Lancet* **1998**, *352*, 673−681.
(49) Young, E.; Venner, T.; Ribau, J.; Shaughnessy, S.; Hirsh, J.; Podor, T. The Binding of Unfractionated Heparin and Low Molecular Weight Heparin to Thrombin-Activated Human Endothelial Cells. *Thromb. Res.* **1999**, *96*, 373−381.
(50) Letourneur, D.; Caleb, B. L.; Castellot, J. J., Jr. Heparin Binding, Internalization and Metabolism in Vascular Smooth Muscle Cells: II. Degradation and Secretion in Sensitive and Resistant Cells. *J. Cell. Physiol.* **1995**, *165*, 687−695.
(51) Li, X.; Zheng, Z.; Li, X.; Ma, X. Unfractionated Heparin Inhibits Lipopolysaccharide-Induced Inflammatory Response Through Blocking p38 MAPK and NF-κB Activation on Endothelial Cell. *Cytokine* **2012**, *60*, 114−121.
(52) Ettelaie, C.; Fountain, D.; Collier, M. E.; Elkeeb, A. M.; Xiao, Y. P.; Maraveyas, A. Low Molecular Weight Heparin Downregulates Tissue Factor Expression and Activity by Modulating Growth Factor Receptor-Mediated Induction of Nuclear Factor-κB. *Biochim. Biophys. Acta* **2011**, *1812*, 1591−1600.
(53) Li, L.; Rui, X.; Liu, T.; Xu, G.; He, S. Effect of Heparin-Derived Oligosaccharide on Vascular Smooth Muscle Cell Proliferation and the Signal Transduction Mechanisms Involved. *Cardiovasc. Drugs. Ther.* **2012**, *26*, 479−488.
(54) Bagel'ova, J.; Antilik, M.; Bona, M. Studies on Cytochrome C−Heparin Interactions by Differential Scanning Calorimetry. *Biochem. J.* **1994**, *297*, 99−101.
(55) Mitsi, M.; Forsten-Williams, K.; Gopalakrishnan, M.; Nugent, M. A. A Catalytic Role of Heparin Within the Extracellular Matrix. *J. Biol. Chem.* **2008**, *283*, 34796−34807.